International Journal of Science and Technology (IJST)
ISSN: 3049-1118, Volume- 3, Issue- 2 (April - June 2026)

Efficiency of Magadiitic Aluminosilicate Nanozeolites for the Removal of Nitrate (NO_3^-) and Phosphate (PO_4^{3-}) Agro-pollutants from Aqueous Solutions

Janes Bochaberi Omoko[1], Njagi Njomo[1], Deborah A. Abong'o[1], Dickson M. Andala[2]
[1] Department of chemistry, Faculty of Science &Technology, University of Nairobi, P.O. Box 30197-00100, Nairobi, Kenya
[2] Department of chemistry, Multimedia University of Kenya, Nairobi P.O. Box 15653- 00503, Nairobi, Kenya

ABSTRACT

The aim of this study was to determine the efficiency of the Magadiitic aluminosilicate nanozeolites in the removal of the agro-pollutants nitrate (NO_3^-) and phosphate (PO_4^{3-}) from aqueous solutions. The findings demonstrated that the optimized nanozeolite exhibited exceptional efficiency and high selectivity for (PO_4^{3-}) ions, achieving removal efficiencies up to or exceeding 99.9 % in optimized specific condition across analysed concentrations ranging from 5 mg/L - 50 mg/L and maintaining nearly perfect removal of 99.999 % across the stable pH range of 2–6. This robust performance for phosphate was linked to strong chemisorption mechanisms, such as ligand exchange and inner-sphere complexation, characterized by a highly spontaneous, ΔG^o= -20.37 kJ/mol at 25 °C and entropy-driven thermodynamic profile, and yielding a maximum adsorption capacity (q_m) of up to 2,736 mg/g. In stark contrast, nitrate removal efficiency was significantly lower and less consistent, ranging between 65.88 % and 71.6 % across concentration changes, and was highly sensitive to increases in pH above 6 and temperature changes above 35 °C. Nitrate adsorption was predominantly confirmed as a physisorption-driven process supported by weaker electrostatic attractions, indicated by a low mean adsorption energy (E) of 3.45 kJ/mol and a less spontaneous nature, ΔG^o= - 6.11 kJ/mol at 25 °C. However, the adsorption kinetics for both anions were best fitted by the Pseudo-Second-Order model, which unequivocally confirmed chemisorption as the overall primary mechanism.

Keywords: Agro-pollutants, Magadiitic aluminosilicate nanozeolite, chemisorption, nitrates, phosphates, physisorption

1. INTRODUCTION

The excessive application of fertilizers and pesticides in agriculture, designed to boost production, is a significant driver of environmental pollution, contributing to soil acidification, greenhouse gas emissions, and widespread water contamination [1]. Specifically, nitrate

Published: 30 June 2026
DOI: https://doi.org/10.70558/IJST.2026.v3.i2.241298

(NO_3^-) and phosphate (PO_4^{3-}) from fertilizers are primary causes of eutrophication in both marine and freshwater environments, while high nitrate concentrations in drinking water pose serious health risks, including methemoglobinemia ("blue baby syndrome") in infants [2]. Despite the clear need for pollution mitigation, research into environmental health and safety has shown minimal focus on utilizing nanotechnology-based zeolite adsorbents for water purification. This research, therefore, aimed to address this critical knowledge gap by exploring the adsorption efficacy of magadiitic aluminosilicate nanozeolites as a cost-effective solution for the removal of pollutants, such as nitrates and phosphates resulting from agricultural chemical overuse, or from agricultural runoff in aquatic system. This investigation aligns directly with the objectives of sustainable agriculture and water management in relation to bottom-up economic transformation agenda, Kenya, seeking to establish effective and affordable methods to reduce environmental contamination.

2. LITERATURE

Chemical contaminants originating from sources like domestic wastes, farm chemicals, and food processing plants pose serious health risks to humans, often being carcinogenic and leading to conditions such as cancer, hormonal problems, and deoxyribonucleic acid (DNA) damage [3]. Furthermore, nutrient pollution, driven by excess nitrogen and phosphates, promotes the overgrowth of toxic algae, resulting in disease outbreaks and death within marine ecosystems [4]. Given this severity, the consumption of inadequately treated or untreated water contaminated by these chemical or nutrient pollutants introduces significant health risks, including the risk of death, which prompted the World Health Organization (WHO) in 2013 to emphasize the urgent global need for access to safe and affordable treated water [5]. Zeolites are identified as highly effective adsorbents for water treatment due to their unique structural features, such as internal channels and chambers, which grant them exceptional physicochemical properties, including remarkable adsorption [6]. These characteristics allow zeolites to be utilized for studying osmotic gradients and for the adsorption of heavy metal ions, organic and inorganic pollutants, and free radicals [7], with the Si: Al ratio in the structure influencing their affinity for different molecules [8].

The remediation of nitrates and phosphates from aqueous environments is a critical focus in water treatment research, primarily driven by the necessity to mitigate eutrophication. A wide array of adsorbents has been investigated, each possessing distinct mechanisms and efficiencies. Conventional activated carbon typically exhibits limited affinity for these oxyanions unless it undergoes chemical modifications, such as amination or impregnation with metal oxides, to enhance its capacity [9]. Biochar has emerged as a sustainable alternative derived from biomass pyrolysis, showing particular promise when engineered with magnesium or lanthanum to facilitate phosphate removal via precipitation and ligand exchange [10], for targeted phosphate sequestration, metal hydroxides/oxides especially those of iron, aluminium, and lanthanum are effective due to strong inner-sphere complexation, though their performance is notably pH-dependent [11].

Layered double hydroxides (LDHs) are considered versatile, capable of adsorbing both nitrates and phosphates through anion exchange and reconstruction effects, although their selectivity may be compromised by competing anions like sulfate [12]. While ion exchange resins,

particularly strong-base anion exchangers, offer high nitrate capacities and fast kinetics, their widespread application is limited by high costs and sensitivity to competing ions [9]. Recent trends in the literature emphasized the development of hybrid and composite materials, such as biochar functionalized with LDHs or metal nanoparticles, to synergized components and improved selectivity, capacity, and regenerability [13]. Despite these advancements, significant challenges persist regarding long-term stability, potential secondary pollution from modified adsorbents, and the economic scalability of advanced materials in real-world water matrices [14]. This study, therefore, aimed to explore the adsorption efficacy of magadiitic aluminosilicate nanozeolites as a cost-effective solution for the removal of pollutants, such as nitrates and phosphates resulting from agricultural chemical overuse, or from agricultural runoff into aquatic system.

3. MATERIALS AND METHODS

3.1 Preparation of Magadiitic aluminosilicate nanozeolite for adsorption.

The production process of Magadiitic aluminosilicate nanozeolite material [15], involved preparation of aluminium sulphate solution; prepared by dissolving 666 g of aluminium sulphate octadecahydrate ($Al_2(SO_4)_3.18H_2O$) in 500 mL of distilled deionized water. The solution was then diluted to one litre using distilled deionized water. A saturated one-litre solution of magadiitic salt was prepared by dissolving 500 g of crushed natural magadiitic salt composite sample SA-02; obtained from Lake Magadi, Kenya in 100 mL warm distilled deionized water, subsequently diluted to one litre. The key step in designing particles involved addition of 200 mL of aluminium sulphate solution (containing 133.5 g) to 1000 mL of magadiitic salt solution resulted in the formation of a solution with pH between 4.7 and 7.7. These led to the precipitation of aluminium silicate nanozeolite. Following precipitation, this material was filtered using a Lab Recessed Chamber Filter Press and the product was washed with distilled deionized water to remove impurities such as unreacted metal silicate and sodium sulphate. The filtered cake was then dried using a flash dryer at an inlet temperature of 350 °C and an outlet temperature of 120 °C. The dried Magadiitic aluminosilicate nanozeolite material was then milled to an average particle size of 1-15µm using a ball mill [15]. The final product, magadiitic aluminosilicate nanozeolite sample AP-05-02 was stored for later use in laboratory analysis.

3. 2 Preparation of nitrate and phosphate stock standard solutions for the studies

Stock solutions of nitrate-nitrogen and phosphate-phosphorous standards were prepared by weighing 1.6306 g of potassium nitrate (KNO_3) and 1. 648 g of dipotassium phosphate (K_2HPO_4) salts, dried in Gallenkamp oven at 105 °C for two hours in 100 mL beaker and each then transferred to a one-liter volumetric flask to make 1000 ppm nitrate and phosphate stock standard solutions respectively.

3.2.1 The Preparation of nitrate and phosphate standard calibration curves

Standard calibration curves for the nitrate and phosphate ions were obtained by measuring absorbance of the stock solutions prepared for nitrates and phosphate anions concentrations using UV-VIS spectrophotometer (uv-vis 190-1100nm Meubon).

The solution of nitrate and phosphorous standard solutions were made for 5 mg/L to 50 mg /L by taking the prepared required standard solution volume in a conical flask.

The nitrates standards solutions were each measured calorimetrically by taking 10 mL of 5 % (w/v) salicylic acid (5 g salicylic acid in 95 mL Sulphuric acid) and adding to the required measured standard solutions in 250 mL volumetric flask then mixed thoroughly by hand shaking. The mixtures were left to settle at room temperature for 30 minutes before slowly adding 100 mL solution of 4 M sodium hydroxide. The mixtures were each again shaken and left to stand for 1 hour. The absorbance was measured using a UV-VIS spectrophotometer at wavelength of 419 nm.

The phosphates standards solutions were measured calorimetrically by taking each required measured standard solution in a 50 mL volumetric flask, then 10 mL of Olsen solution (0.5 M sodium bicarbonate ($NaHCO_3$) solution adjusted to a pH of 8.5) was added followed by 20 mL distilled deionized water, and 8 mL of Murphy Riley solution then made to 50 mL using distilled deionized water and analyzed using a UV-VIS spectrophotometer at 882 nm wavelength. The level of total phosphorous in water samples expressed in mg/L were calculated using equations 1 and 2.

The relationship of concentration of nitrate and phosphate anion by absorbance gave a regression line equation $y = mx + c$. The regression equation was used to determine the concentration of nitrate and phosphate anions in the aqueous system.
Percentage removal of nitrate and phosphate from aqueous system was calculated using the Equation 1

$$\% \text{ Removal} = \frac{(C_0 - C_e)}{C_0} 100 \quad \text{.....Equation 1}$$

where C_0 = initial concentration of nitrate/phosphate anion and C_e is the final concentration.
Adsorption capacity (q_e) after reaching equilibrium was calculated using the Equation 2

$$\text{Adsorption capacity } (q_e) = (C_0 - C_e)\frac{V}{W} \quad \text{..... Equation 2}$$

where V is volume (L) of solution and W is the mass (g) of adsorbent used.

3.3 Adsorption of nitrates and phosphates anions onto magadiitic aluminosilicate nanozeolite

Adsorption characteristics were conducted based on percentage adsorption, by varying pH, concentration, temperatures, adsorbent mass and contact time. The batch experiments were conducted at optimum conditions that influenced NO_3^- and PO_4^{3-} ions adsorption as well as their adsorption isotherms, kinetics and thermodynamic parameters. The optimum conditions determined were adsorbent dosage, initial ion concentration, temperature, pH and contact time. Various adsorbent dosage of 0.005 g, 0.01 g, 0.015 g, 0.02 g and 0.03 g of magadiitic aluminosilicate nanozeolite were each shaken with 10 mL of 5 mg/L, 10 mg/L, 25 mg/L and 50 mg/L of NO_3^- and PO_4^{3-} ions solution at 100 rpm, at different temperature; using a water bath at 20 °C, 25 °C, 35 °C, 45 °C and 50 °C representing 293 K, 298 K, 308 K, 318 K and 323 K respectively and the pH range of 2, 4, 6, 8 and 10. The determination on the effects of contact time was carried out on the adsorption of NO_3^- and PO_4^{3-} ions at regular time different contact intervals time of 15, 30, 45 and 60 minutes, then each analytical sample was filtered

using standard sieve 0.3 mm IS sieves and analysed, all the analyses were done in triplicate. The amount of NO_3^- and PO_4^{3-} ions adsorbed were analysed using a UV-VIS spectrophotometer at 419 and 882 nm wavelength respectively and the difference between the final (C_e) and initial concentrations (C_0) were used to calculate percentage adsorption using Equation 1. The results were compared with documented data of clinoptiolite which was used as a standard commercial aluminosilicate nanozeolite**.** Optimum conditions determined above are specific environmental and system parameters that maximize the anion adsorption efficiencies for a given adsorbent. These conditions directly influence the mechanisms and efficiency of adsorption process, which in turn dictated the best-fit Isotherm and kinetic model and the resulting thermodynamic parameters of that process. Langmuir, Freundlich, Temkin, Dubinin-Radushkevich kinetic models' studies and adsorption thermodynamics were implemented to equilibrium results obtained to show the efficiency of the developed Magadiitic aluminosilicate nanozeolite material [15] in the removal of NO_3^- and PO_4^{3-} ions from aqueous solutions.

3.4 Adsorption Isotherm models

Adsorption Isotherms of NO_3^- and PO_4^{3-} anions were analyzed by applying the Langmuir, Freundlich, Temkin and Dubinin-Radushkevich models.

3.4.1 Langmuir Isotherm

Langmuir Isotherm [16] describes a monolayer adsorption of adsorbent by assuming that all sites are energetically identical. It was given by Equation 3

$$\frac{C_e}{q_e} = \frac{1}{k_l Q_o} + \frac{C_e}{Q_o}, \quad R_L = \frac{1}{1+k_l C_o} \qquad \text{..... Equation 3.}$$

In Langmuir Isotherm, R_L is a dimensionless separation factor or equilibrium parameter used to determine the favorability of an adsorption process.

Where the R_L values show the type of Isotherm ($0 < R_L < 1$ (favorable), $R_L > 1$(unfavorable), $R_L = 0$ (irreversible) and $R_L = 1$ (linear)

3.4.2 Freundlich Isotherm

Adsorption on heterogeneous surfaces is described by Freundlich Isotherm [17] which is formulated and obtained from Equation 4

$$Inq_e = In\mathrm{k} + \frac{1}{n} InC_e \qquad \text{..... Equation 4}$$

3.4.3 Temkin Isotherm

Temkin Isotherm [18] model assumes linear decrease of adsorption heat of all molecules and uniform distribution of binding energies. B which is a constant related to the heat of adsorption and is defined by the expression B=RT/b. It is described by Equation 5

$$q_e = \frac{RT}{b} InC_e + \frac{RT}{b} InK_T \qquad \text{.....Equation 5}$$

In the Temkin Isotherm model B is a constant related to the heat of adsorption. It indicates how the adsorption energy changes with surface coverage, representing the energy of sorption.

3.4.4 Dubinin-Radushkevich (D-R) Isotherm

Dubinin-Radushkevich (D-R) Isotherm [19] model considers the influence by temperature and micropore size on adsorption. It is expressed using the adsorption potential ε using Equation 6

$$\varepsilon = \mathrm{RT}\, In(1 + \frac{1}{\mathrm{C_e}}) \quad \text{..... Equation 6}$$

A Gaussian type distribution of D-R Isotherm can be calculated using Equation 7

$$In\ q_e = In\ q_s - \beta\varepsilon^2 \quad \text{..... Equation 7}$$

Where q_s is the D-R constant ($molg^{-1}$) and β is a constant related to adsorption energy; the mean adsorption energy E ($kJmol^{-1}$) per molecule of adsorbate at the moment of its transfer to the solid surface from the bulky solution is computed using Equation 8.

$$\mathrm{E} = \frac{1}{(2\beta)^{1/2}} \quad \text{..... Equation 8}$$

The mean adsorption energy, E, shows the nature of adsorption process such as chemical ion exchange or physical adsorption. If the value is smaller than 8 kJ/mol, then the reaction continues physically [20]. When the value is more than 8 kJ/mol, then the process will proceed chemically.

3.5 Kinetic studies

Lagergren Pseudo first and second–order kinetic models [21] were used in the study. Pseudo first-order kinetic is given by Equation 9

$$In\ (q_e - \mathrm{q_t}) = In\ \mathrm{q_t} - \mathrm{K_1 t} \quad \text{..... Equation 9}$$

Pseudo second-order kinetic model is given by Equation 10

$$\frac{t}{\mathrm{q_t}} = \frac{1}{\mathrm{K_2}\ q_e{}^2} + \frac{t}{\mathrm{q_e}} \quad \text{..... Equation 10}$$

3.6 Adsorption Thermodynamics

Thermodynamic parameters which include Gibbs free energy (ΔG^o), enthalpy changes (ΔH^o) and entropy change (ΔS^o) were determined. Gibbs free energy was calculated using the Equation 11

$$\Delta G^o = -\mathrm{RT\ In K_a} \quad \text{..... Equation 11}$$

The ΔH^o and ΔS^o were determined using Van't Hoff's plot calculated using Equation 12

$$\mathrm{In K_a} = \Delta H/RT + \Delta S/R \quad \text{..... Equation 12}$$

4. RESULTS AND DISCUSSION

4.1 Optimal conditions for nitrates and phosphate adsorptions on Magadiitic Aluminosilicate nanozeolite

4.1.1 Effect of pH on adsorption of nitrates and phosphates anions

The effect of pH on nitrate (NO_3^-) and phosphate (PO_4^{3-}) adsorption across the range of 2–10 (Figure 1) revealed distinct behaviors for each anion, despite both achieving very high removal efficiency of > 99.65 % for NO_3^- and > 99.96 % for PO_4^{3-} (Table 1)

Table 1: Effect of pH on nitrate and phosphate anions adsorption.

pH	% Adsorption (PO_4^{3-})	% Adsorption (NO_3^-)
2	99.9992	99.976
6	99.9992	99.936
8	99.9924	99.904
10	99.964	99.656

Phosphate adsorption was consistent and highly pH-resistant, showing a near-perfect plateau at pH 2–6 (slope = 0) where maximum removal of ≥ 99.999 % was maintained, suggesting that the magadiitic aluminosilicate nanozeolite adsorbent was highly effective even at alkaline pH ≥ 8 (Table 1). This exceptional stability was linked to the dominance of ligand exchange mechanisms, where PO_4^{3-} forms strong inner-sphere complexes that are less pH-dependent [22], with only a minor drop in efficiency occurring above pH 8, likely due to competition with hydroxyl ions [23]. Conversely, nitrate adsorption showed greater variability and sensitivity to pH increases, exhibiting a high-stability near-plateau only between pH 2–6. Beyond pH 6, the decline in nitrate removal efficiency steepened considerably, falling to 99.656 % at pH 10, because nitrate adsorption primarily occurs through outer-sphere electrostatic attractions that are highly susceptible to pH-induced surface charge changes [9]. Consequently, while no pH adjustment was necessary for efficient PO_4^{3-} removal across the entire pH range, optimal performance for NO_3^- removal required maintaining acidic conditions (pH ≤ 6) (Figure 1).

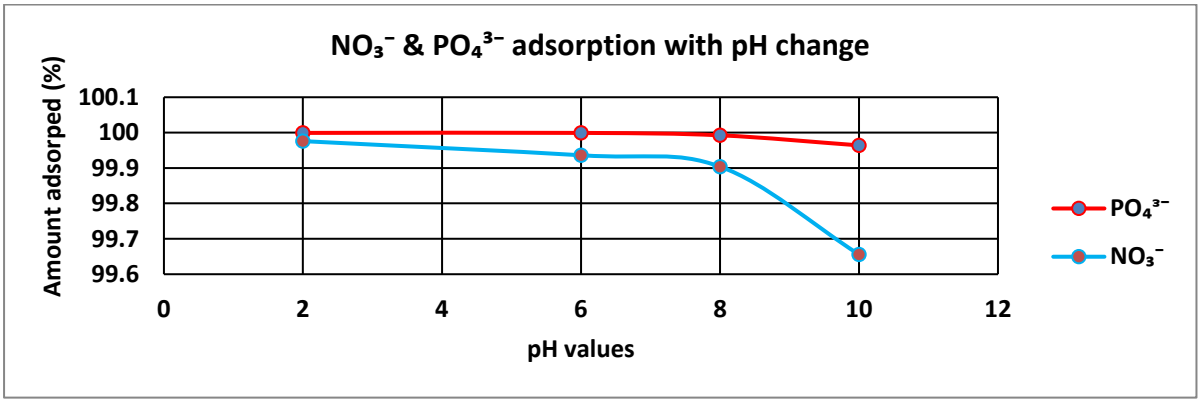

Figure 1: The effect of pH on adsorption of nitrate (NO_3^-) and phosphate (PO_4^{3-}) anions

4.1.2 The effects of concentration on nitrate and phosphate adsorption

The effect of concentration on percentage adsorption efficiency differed between nitrate (NO_3^-) and phosphate (PO_4^{3-}) anions onto the magadiitic aluminosilicate nanozeolite adsorbent. Phosphate adsorption demonstrated exceptional stability and efficiency across the used initial concentrations, ranging from 5 mg/L to 50 mg/L, with removal efficiencies consistently exceeding 99.9 % (Table 2)

Table 2: The effects of concentration on nitrate and phosphate adsorption

	% adsorption onto magadiitic aluminosilicate nanozeolite	
mg/L	% PO_4^{3-}	% NO_3^-
5	99.994	71.6
10	99.993	68.6
25	99.9692	65.88

50	99.9276	67.52

This performance showed minimal decrease in efficiency, from 99.994 % at 5 mg/L to 99.9276 % at 50 mg/L (Figure 2) reinforcing its high affinity; this stability was evidenced statistically by an extremely low range of 0.0664 % and the observation of a clear saturation plateau within the used concentration range. This near-quantitative removal was attributed to strong chemisorption mechanisms like electrostatic attraction and ligand exchange, which dominate phosphate uptake regardless of concentration changes [24]. In contrast, nitrate adsorption was significantly lower and less consistent, ranging only between 65.88 % and 71.6 % (Table 2). Nitrate uptake did not show a clear trend across increasing concentrations, nor did it reach a clear saturation plateau within the 5–50 mg/L range (Figure 2). This higher variability (range of 5.72 %) was primarily attributed to weaker electrostatic attraction compared to multivalent phosphate ions [25], as well as competitive adsorption effects from other anions in the solution interfering with nitrate removal.

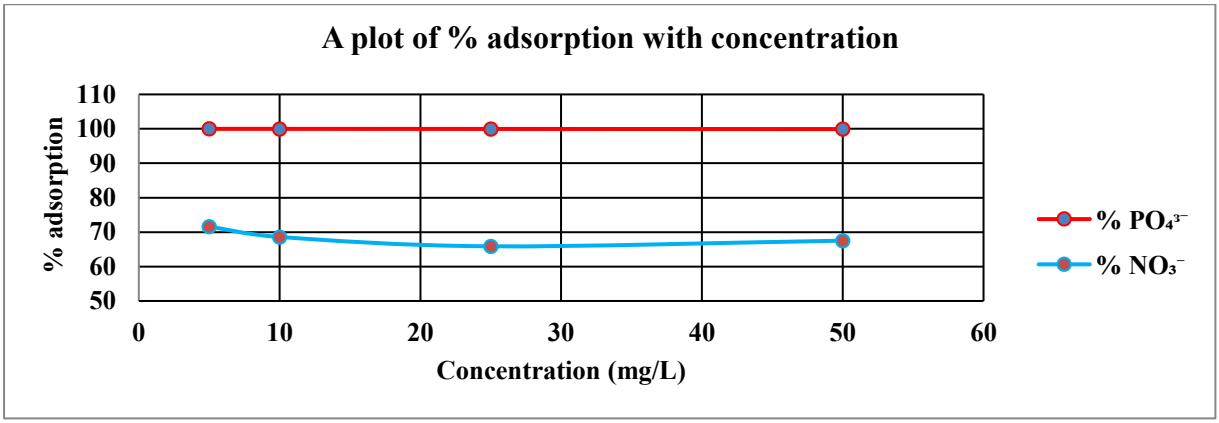

Figure 2: Percentage adsorption of PO_4^{3-} and NO_3^- anions with change in concentration

4.1.3 Effect of Temperature on adsorption of nitrate and phosphate anions

Temperature profoundly affects the adsorption of nitrate (NO_3^-) and phosphate (PO_4^{3-}) ions on magadiitic aluminosilicate nanozeolite, demonstrating distinct dependencies across the studied temperature range of 20 °C to 50 °C (Table 3).

Table 3: Effect of temperature on the adsorption of PO_4^{3-} and NO_3^- anions

Temperature (°C)	% adsorption of PO_4^{3-}	% adsorption of NO_3^-
20	99.236	89.4
25	99.997	91.7
30	99.997	91.72
45	99.996	86.16
50	99.994	86.04

Phosphate adsorption exhibited remarkable temperature stability and efficiency, consistently achieving over 99.2 % removal across the entire range (Figure 3). The maximum adsorption efficiency of 99.997 % was achieved at 25 °C and sustained up to 35 °C (Table 3) with this consistent high performance attributed to strong chemisorption mechanisms that were largely

insensitive to temperature changes [26]. A slight observed decrease in phosphate adsorption efficiency occurred only at the highest temperatures (45 °C to 50 °C), potentially suggesting minor desorption effects or weakened electrostatic attractions [27]. In stark contrast, nitrate adsorption exhibited greater temperature sensitivity and variability, showing characteristics of physisorption or weak chemisorption. Nitrate removal initially increased from 20 °C up to an optimal efficiency of 91.72 % occurring at 35 °C (Table 3) suggesting an endothermic process where enhanced temperature aids kinetics and nitrate mobility [9]. However, beyond this optimal point, nitrate adsorption significantly declined, showing a 5.7 % drop between 35 °C and 50 °C (Figure 3), which is likely due to the weakening of physical adsorption forces at elevated temperatures [25]. These distinct temperature responses underscored fundamental differences in adsorption mechanisms, where phosphate's robust removal was suitable for various conditions, while nitrate's temperature sensitivity implied that process optimization was required for consistent performance in diverse climatic conditions [9]

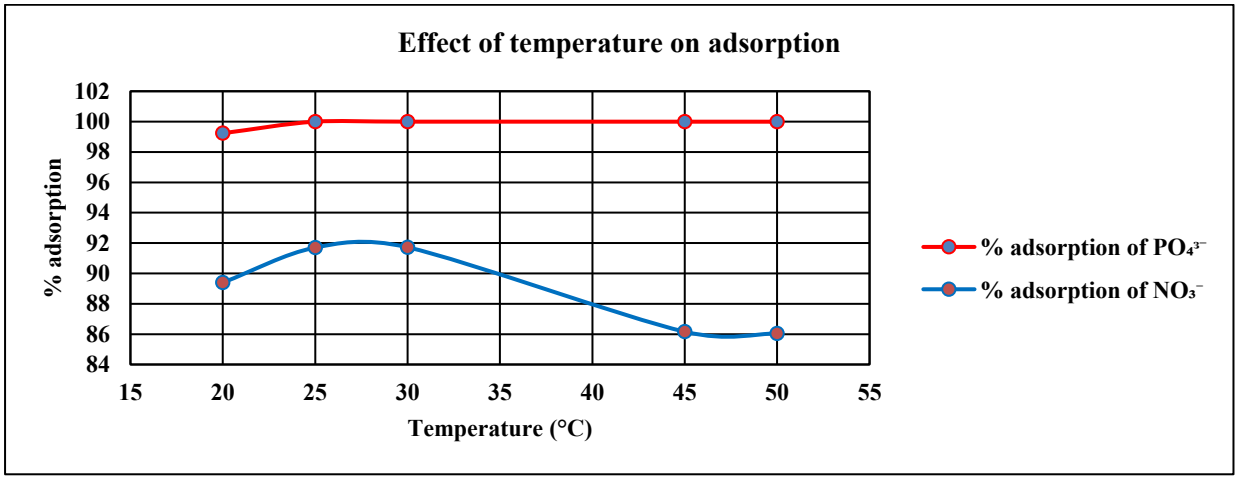

Figure 3: The percentage adsorption effects of temperature on nitrate and phosphate anions

4.1.4 Effect of adsorbent mass on phosphate (PO_4^{3-}) and nitrate (NO_3^-) anions adsorption

The mass of the Magadiitic aluminosilicate nanozeolite adsorbent demonstrated a strong influence on the adsorption efficiency for both phosphate (PO_4^{3-}) and nitrate (NO_3^-) ions, with phosphate removal proving far more efficient at lower dosages. For phosphate, the nanozeolite exhibited a strong inherent affinity, achieving high efficiency of 94.02 % even at the minimal mass of 0.001g (Table 4).

Table 4: Effect of adsorbent mass on percentage phosphate (PO_4^{3-}) and nitrate (NO_3^-) anion adsorption

Mass g	% adsorption PO_4^{3-}	% adsorption NO_3^-
0.001	94.02	76.41
0.002	99.9744	83.06
0.005	99.984	88.876
0.01	99.9876	91.544
0.02	99.988	91.919
0.03	99.989	91.93

Increasing the mass to 0.002 g caused the efficiency to rise sharply to 99.9744 %, signifying that the adsorption was nearing saturation and leading to the identification of 0.002 g as the optimal, cost-efficient dose for near-total PO_4^{3-} removal (Figure 4), as further mass increases up to 0.03 g resulted in only marginal improvements peaking at 99.989 % (Table 4). In contrast, nitrate adsorption efficiency was comparatively lower, starting at 76.41% at 0.001 g, suggesting a weaker affinity or presence of competition for adsorption sites [9]. Nitrate (NO_3^-) ions removal was notably mass-dependent and necessitated higher doses to achieve comparable removal percentages (Table 4), showing significant improvements up to 0.01 g. However, NO_3^- ions removal did not achieve near-complete saturation, instead plateauing at approximately 91.93 % even at the maximum tested mass of 0.03 g (Figure 4), indicating limitations in binding capacity linked to the nanozeolites' lower selectivity for the monovalent anion [25].

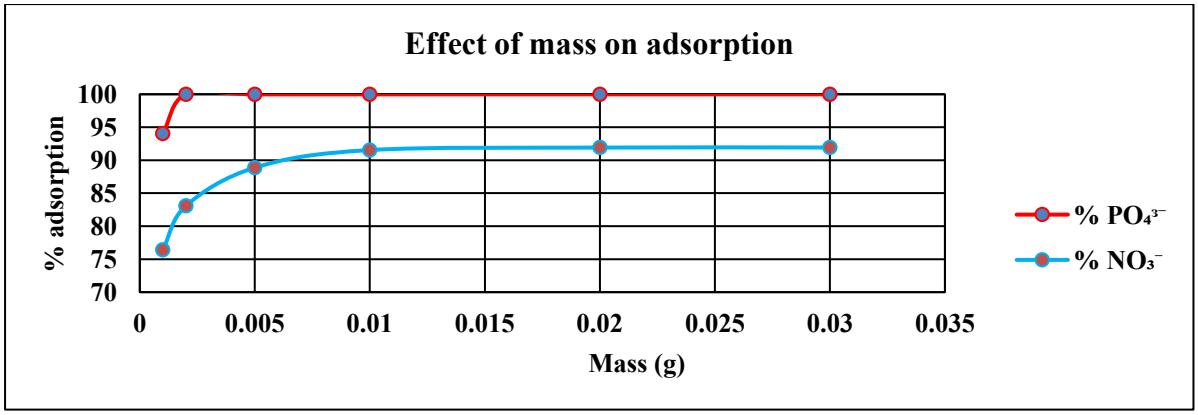

Figure 4: Effect of adsorbent mass on the percentage phosphate (PO_4^{3-}) and nitrate (NO_3^-) anions

4.1.5: Effect of contact time on phosphate (PO_4^{3-}) and nitrate (NO_3^-) anions adsorption

The adsorption efficiency of anions using magadiitic aluminosilicate nanozeolite is strongly dependent on contact time, revealing that phosphate (PO_4^{3-}) and nitrate (NO_3^-) exhibit contrasting kinetics (Table 5).

Table 5: Effect of contact time on the adsorption of phosphate (PO_4^{3-}) and nitrate (NO_3^-) anions

Time (Min)	% adsorption PO_4^{3-}	% adsorption NO_3^-
15	96.8968	91.7384
30	99.9712	95.064
45	99.984	95.0752
60	99.9876	95.16
75	99.994	95.17

Initially, a rapid adsorption phase occurs between 15 and 30 minutes (Table 5), during which abundant active sites on the nanozeolite surface allow for immediate ion binding, resulting in PO_4^{3-} reaching 96.90 % adsorption and NO_3^- reaching 91.74 % (Figure 5). However, the time required to achieve equilibrium and maximum efficiency varied significantly; PO_4^{3-} adsorption

increased sharply to 99.97 % at 30 minutes and remained nearly constant, approximating to 99.994 % up to 75 minutes, indicating that active sites quickly became saturated and the optimal contact time for near-complete removal was 30 minutes. Conversely, NO_3^- adsorption showed slower, more gradual kinetics, rising from 91.74 % at 15 minutes to 95.17 % at 75 minutes (Table 5), necessitating longer contact times (exceeding 60 minutes) for maximum efficiency. This slower process for NO_3^- was attributed to its weaker affinity for the adsorbent surface or diffusion limitations requiring more time for the ions to access internal adsorption sites within the nanozeolite pores [11].

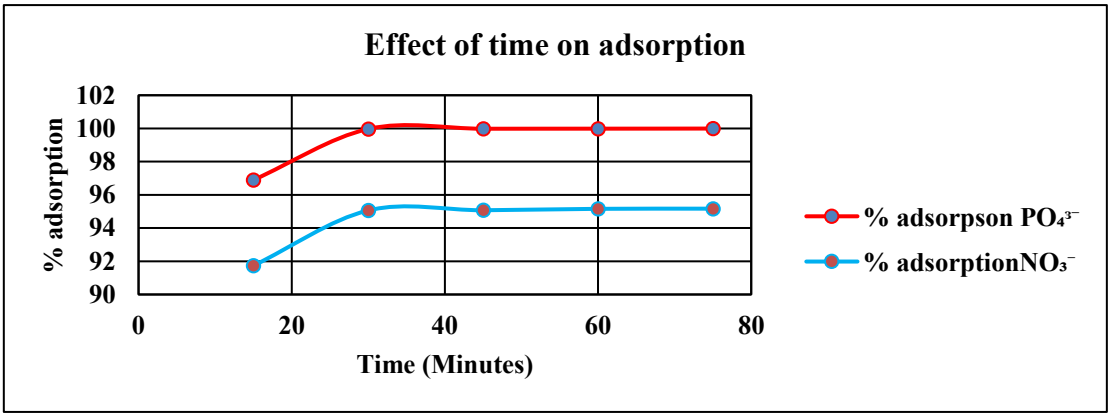

Figure 5: Effect of contact time on the percentage adsorption of PO_4^{3-} and NO_3^- anions

4.2 Adsorption Isotherms

4.2.1 Langmuir adsorption Isotherms for Phosphate (PO_4^{3-}) and Nitrate (NO_3^-) anions

The Langmuir Isotherm model proved effective in describing the adsorption of lead, chromium and cadmium heavy metal ions [28] and for both phosphate (PO_4^{3-}) and nitrate (NO_3^-) in this study on magadiitic aluminosilicate nanozeolite, revealing distinct differences in their adsorption mechanisms and suggesting a homogeneous adsorption process. For PO_4^{3-} adsorption, the model exhibited an exceptionally good fit (Figure 6) with an R^2 value of 0.999, yielding a maximum adsorption capacity (q_m) of 2,500 mg/g, and a very high binding affinity ($K_L = 4.0 \times 10^5$ L/mg) (Table 6), which strongly suggested the dominant adsorption mechanism was chemisorption, potentially involving ligand exchange or inner-sphere complexation [9]. In contrast, the Langmuir model showed only a moderate fit (Figure 7) for NO_3^- with $R^2 = 0.886$, indicating the process might have been heterogeneous and involved multi-layer formation [27]. This moderate fit correlated with a significantly lower K_L value of 26.3 L/mg (Table 6), which is indicative of weaker physisorption mechanisms like electrostatic attraction, even though the q_m for NO_3^- was higher at 5,000 mg/g [25].

Table 6: Comparative Langmuir Isotherm parameters for PO_4^{3-} and NO_3^- anions

Parameter	PO_4^{3-}	NO_3^-
q_m (mg/g)	2500	5000
K_L (L/mg)	4.0×10^5	26.3
R^2	0.999	0.886

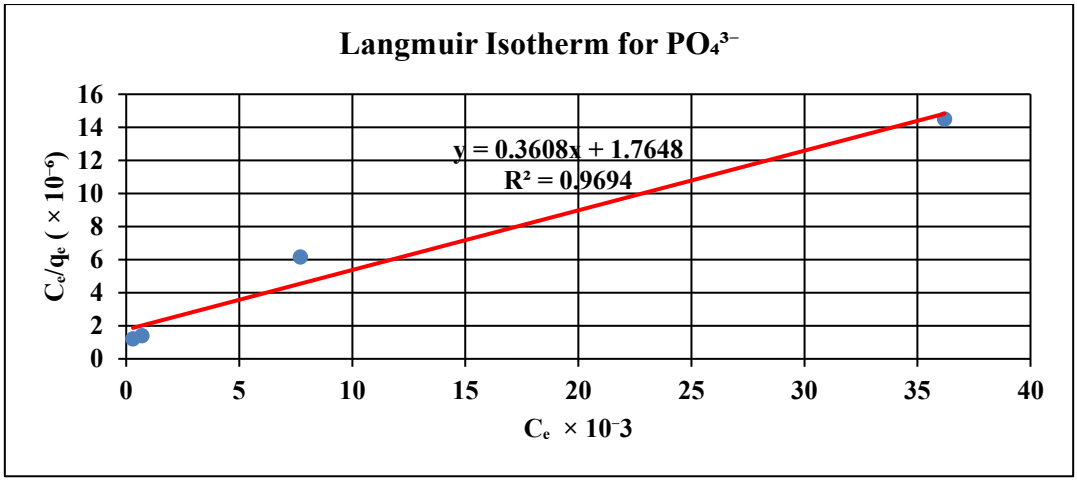

Figure 6: Langmuir adsorption Isotherm for phosphate (PO_4^{3-}) anion

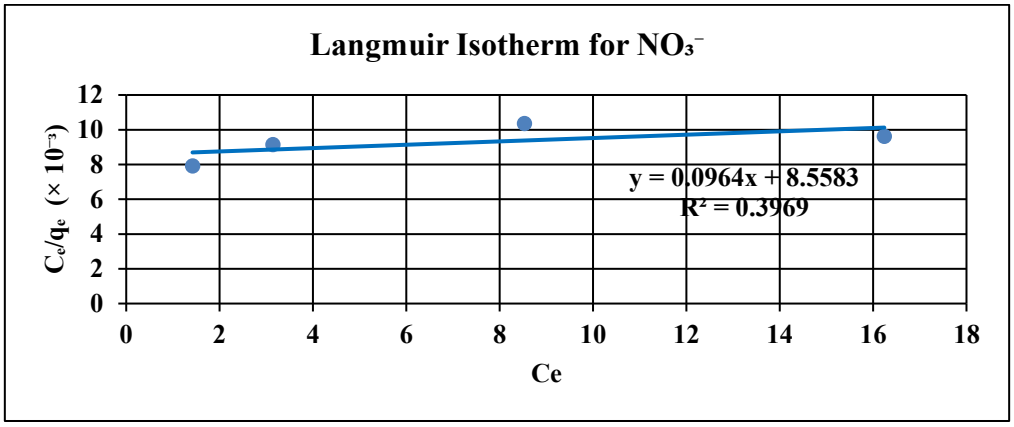

Figure 7: Langmuir adsorption Isotherm for nitrate (NO_3^-) anion

4.2.2 Freundlich adsorption Isotherms for Phosphate (PO_4^{3-}) and Nitrate (NO_3^-) anions The Freundlich Isotherm model used in the analysis of adsorption on magadiitic aluminosilicate nanozeolite provided insight through its capacity parameter (K_F) and intensity parameter (n), yielding an excellent in Figures 8 and 9 that fit for both phosphate with R^2= 0.987 (Figure 8) and nitrate R^2= 0.998 (Figure 9). Analysis of phosphate (PO_4^{3-}) revealed a superior capacity, evidenced by a high K_F of 3020 (L/mg) $^{1/n}$ (Table 7) which significantly surpassed values typically reported for zirconium oxides (120 L/mg - 500 L/mg) [29]. The corresponding n value of 3.23 where n > 1 indicated favorable adsorption and suggested a dominance of chemisorption, likely occurring via ligand exchange, alongside multilayer adsorption on energetically heterogeneous surfaces [24]. Conversely, nitrate (NO_3^-) adsorption showed a moderate capacity, characterized by a lower K_F of 141 mg/g and a mildly favorable n value of 1.22 mg/g, which implied predominantly electrostatic attractions (physisorption) and suggested adsorption sites were less heterogeneous and more uniform than those for phosphate [27]. The substantially lower n value for nitrate, compared to phosphate's 3.23 mg/g, was consistent with its weaker surface attraction as a monovalent anion versus the trivalent phosphate anion, confirming the magadiitic nanozeolites high selectivity for phosphate (Table 7).

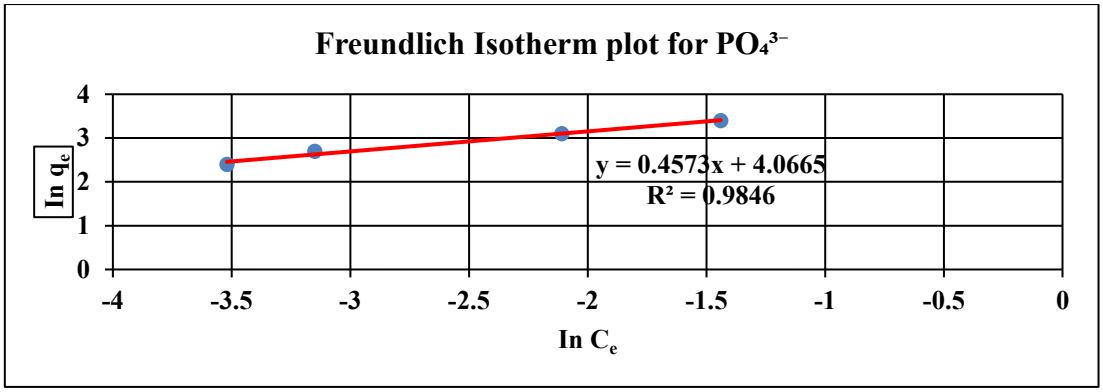

Figure 8: Freundlich adsorption Isotherm for phosphate (PO_4^{3-}) anion

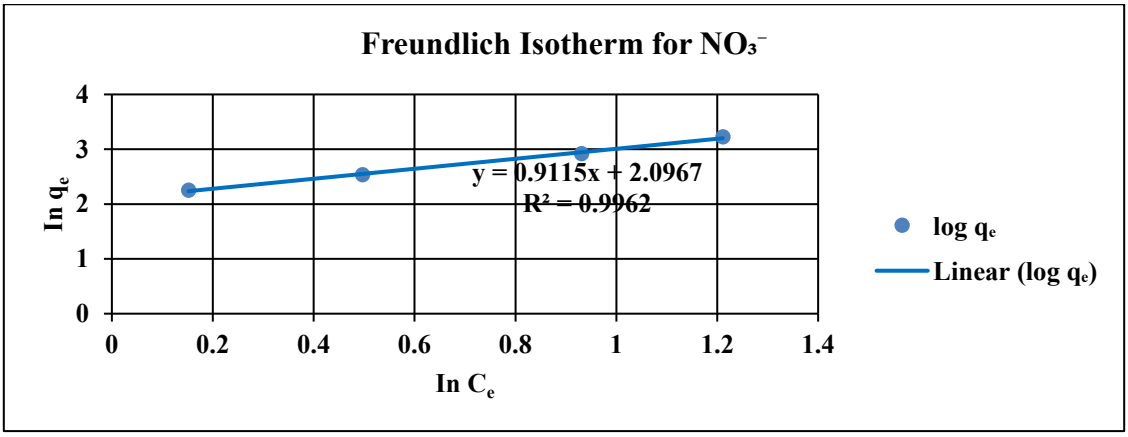

Figure 9: Freundlich adsorption Isotherm for nitrate (NO_3^-) anion.

Table 7: Comparative Freundlich Adsorption Isotherm Parameters for Phosphate and Nitrate anions

Parameter	PO_4^{3-} Value	NO_3^- Value
K_F	3020	141
K_F (Literature range)	120–500	10–100
n	3.23	1.22
R^2	0.987	0.998

Source [29] and [30] respectively

4.2.3 Temkin adsorption Isotherm parameters for Phosphate and Nitrate anions

The analysis using the Temkin adsorption model effectively distinguished the adsorption mechanisms for phosphate (PO_4^{3-}) (Figure 10) and nitrate (NO_3^-) (Figure 11) anions on magadiitic aluminosilicate nanozeolite. For phosphate, the Temkin constant (b) was determined to be 8.30 kJ/mol (Table 8) placing the interaction within the borderline chemisorption range from 8 kJ/mol –16 kJ/mol, signifying strong adsorbate-adsorbent interactions [31]. This strong binding was linked to mechanisms like ligand exchange and the formation of inner-sphere complexes [27]. The corresponding equilibrium constant (A) of 1606 L/mg for phosphate suggested near-irreversible binding, with these high A and b values indicating the adsorbent's superior affinity for PO_4^{3-} when compared to materials like Al-modified clay or ZrO_2 nanoparticles [24]. Conversely, the Temkin constant (b) for nitrate was

significantly lower at 3.52 kJ/mol, a value less than 8 kJ/mol which confirmed that the dominant mechanism was physisorption, such as electrostatic attraction or hydrogen bonding. This weaker interaction resulted in a modest nitrate equilibrium constant (A) of 1.22 L/mg, reflecting reversible adsorption [11]. The pronounced difference where PO_4^{3-} exhibited significantly higher b and A values than NO_3^- justified the material's application for phosphate-selective remediation.

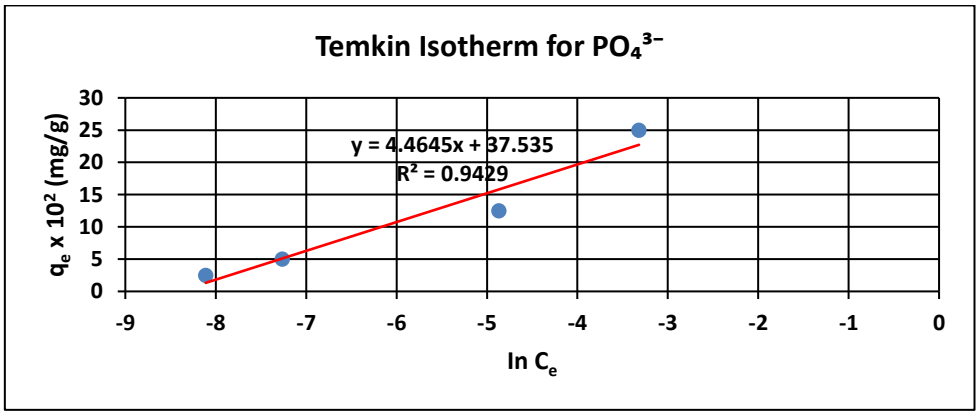

Figure 10: Temkin adsorption Isotherm for phosphate (PO_4^{3-}) anion

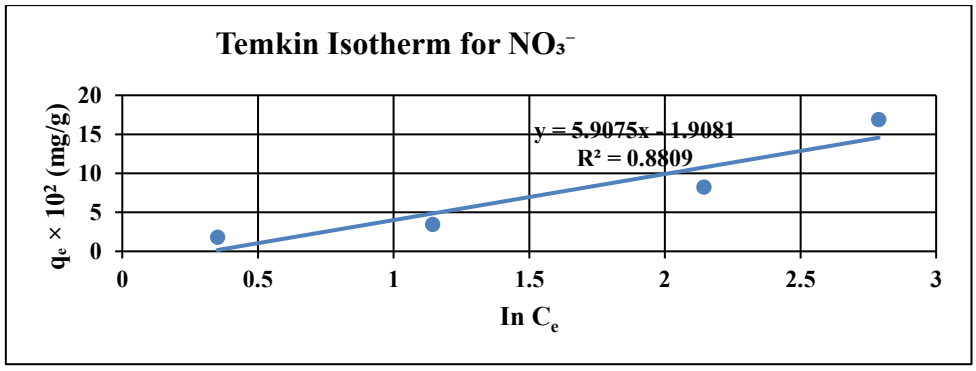

Figure 11: Temkin adsorption Isotherm for nitrate (NO_3^-)

Table 8: Comparative Temkin adsorption Isotherm for Phosphate and Nitrate anions

Anion	Parameter	Value
PO_4^{3-}	*A*	1606 L/mg
	b	8.30 kJ/mol
	R^2	0.943
NO_3^-	*A*	1.22 L/mg
	b	3.52 kJ/mol
	R^2	0.881

4.2.4 D-R adsorption Isotherm parameters for Phosphate and Nitrate anions

The Dubinin-Radushkevich (D-R) Isotherm analysis was utilized to determine the mean free energy (E) and the maximum adsorption capacity (q_m) for both phosphate (PO_4^{3-}) (Figure 12) and nitrate (NO_3^-) (Figure 13) adsorption anions on a magadiitic aluminosilicate nanozeolite. Crucially, the E value was compared against an 8 kJ/mol threshold to distinguish between

physisorption and chemisorption mechanisms. For phosphate, the D-R analysis (Table 9) yielded an E value of 7.58 kJ/mol, suggesting a mixed adsorption mechanism involving primary chemisorption and secondary physisorption [32]. Phosphate's resulting q_m was very high at 2736 mg/g, which surpassed the capacity found using the Langmuir model of 2500 mg/g, pointing toward multilayer adsorption occurring within the material's microporous structure [9]. Conversely, the D-R analysis for nitrate revealed a significantly lower E value of 3.45 kJ/mol, which confirmed that nitrate adsorption was predominantly a physisorption-driven process supported by weak electrostatic attraction and ion exchange [11]. Nitrate's resultant D-R q_m was 456 mg/g, a performance linked to the adsorbent's tuned interlayer spacing [30].

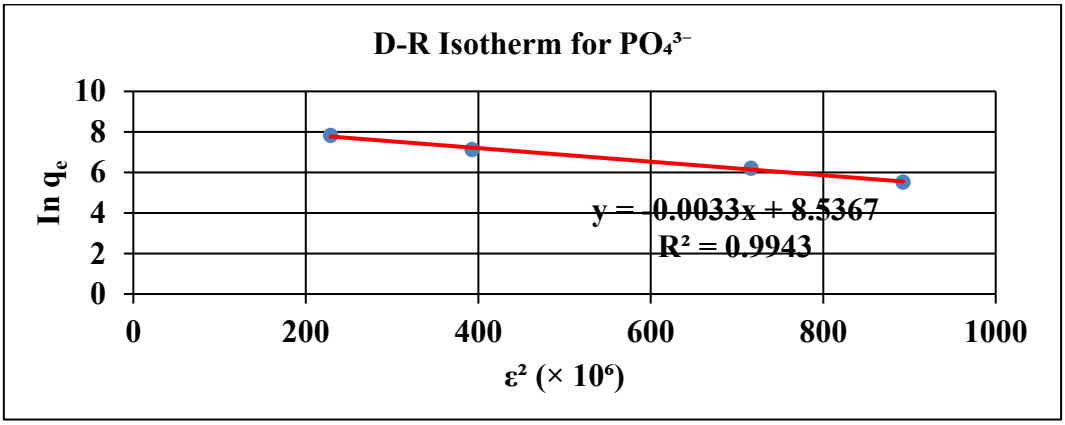

Figure 12: D-R adsorption Isotherm of phosphate (PO_4^{3-}) anion

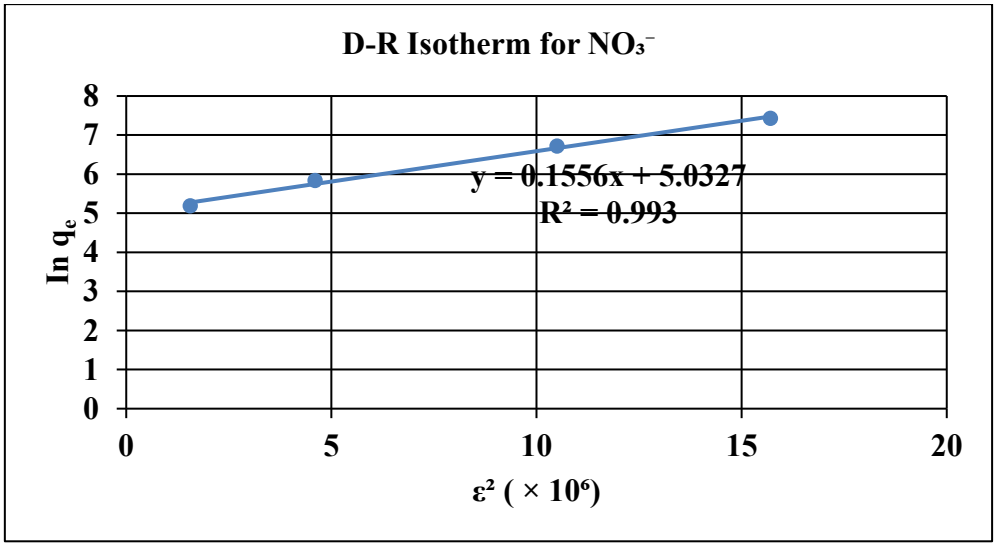

Figure 13: D-R adsorption Isotherm of nitrate (NO_3^-) anion

Table 9: Dubinin-Radushkevich (D-R) adsorption parameters for phosphate (PO_4^{3-}) and nitrate (NO_3^-) anions

Parameter	PO_4^{3-} Value	NO_3^- Value
q_m	2736 mg/g	456 mg/g
β	8.7×10^{-3} mol²/J²	0.042 mol²/J²
E	7.58 kJ/mol	3.45 kJ/mol
R^2	0.994	0.993

4.3 Adsorption kinetics analysis for nitrate (NO_3^-) and PO_4^{3-} anions

The analysis of anion adsorption kinetics for both nitrate NO_3^- and phosphate PO_4^{3-} relied heavily on fitting experimental data to the Pseudo-First-Order (PFO) and Pseudo-Second-Order (PSO) models. For both anions, the PSO model provided a superior fit compared to the PFO model (Figure 14), with the NO_3^- kinetic data showing an excellent PSO fit (Figure 15) R^2 value of 1.0, which confirmed that the adsorption process followed second-order kinetics. This excellent fit using the PSO model for both NO_3^- and PO_4^{3-} (Figures 16 and 17) unequivocally confirmed chemisorption as the primary mechanism, while the poor fit of the PFO model (Figure 14 and 15) suggested the process was not purely diffusion-controlled and effectively ruled out purely physisorption-driven kinetics [33]. While nitrate adsorption approached equilibrium quickly, achieving 95.1 % removal in approximately 30 minutes (Table 10), PO_4^{3-}exhibited faster adsorption kinetics (Table 12), which aligned with its higher charge density; conversely, NO_3^- kinetics is also influenced by diffusivity and competitive effects when studied in multi-ion systems. Practically, the high accuracy of the PSO model was highly valuable for optimizing necessary contact times in adsorption systems (Tables 11 and 13)

Table 10: Pseudo-First-Order (PFO) Model Fitting for nitrate (NO_3^-) anion

Time (min)	(q_t)	(q_e - q_t)	ln (q_e - q_t)
15	91.7384	3.4316	1.2326
30	95.064	0.106	-2.2448
45	95.0752	0.0948	-2.3566
60	95.16	0.01	-4.6052

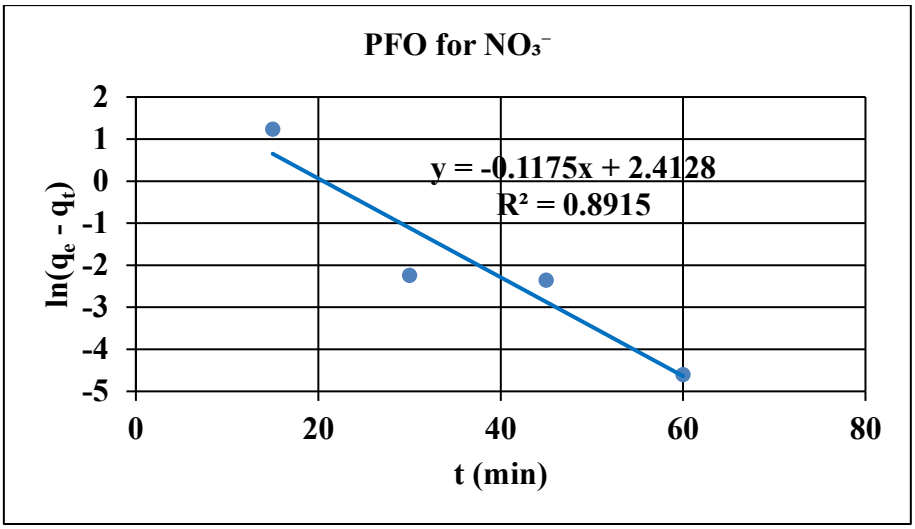

Figure 14: Pseudo-First-Order parameters for nitrate (NO_3^-) anions

Table 11: Pseudo-Second-Order (PSO) Model Fitting for nitrate (NO_3^-) anion

Time (min)	(q_t)	(t/q_t)
15	91.7384	0.1635
30	95.064	0.3156

45	95.0752	0.4733
60	95.16	0.6305
75	95.17	0.7881

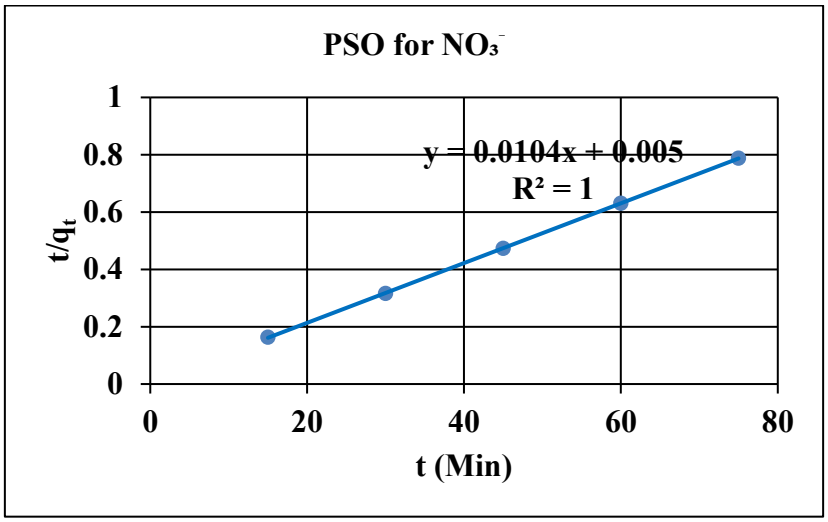

Figure 15: Pseudo-Second-Order parameters for nitrate (NO_3^-) anions

Table 12: Pseudo-First-Order (PFO) Model Fitting for PO_4^{3-} anion

Time (min)	% Adsorption q_t	$(q_e - q_t)$	ln $(q_e - q_t)$
15	96.8968	3.1032	1.1324
30	99.9712	0.0288	-3.5489
45	99.984	0.016	-4.1352
60	99.9876	0.0124	-4.3895
75	99.994	0.006	-5.116

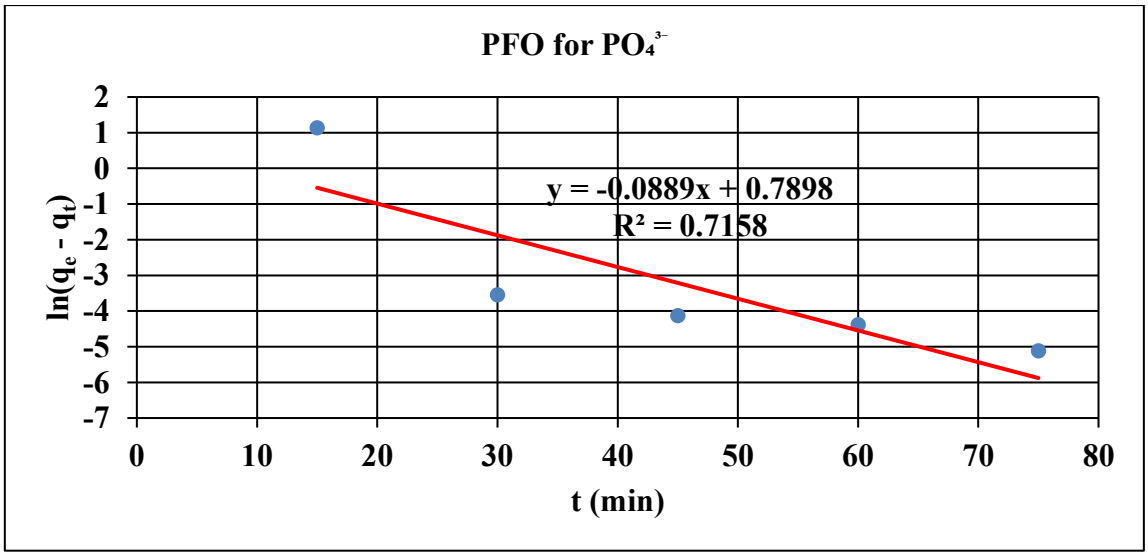

Figure 16: Pseudo-First-Order parameters for phosphate (PO_4^{3-}) anion

Table 13: Pseudo-Second-Order (PSO) Model Fitting for phosphate (PO_4^{3-}) anions

Time (min)	(q_t)	t/q_t
15	96.8968	0.1548
30	99.9712	0.3001
45	99.984	0.4501
60	99.9876	0.6001
75	99.994	0.75

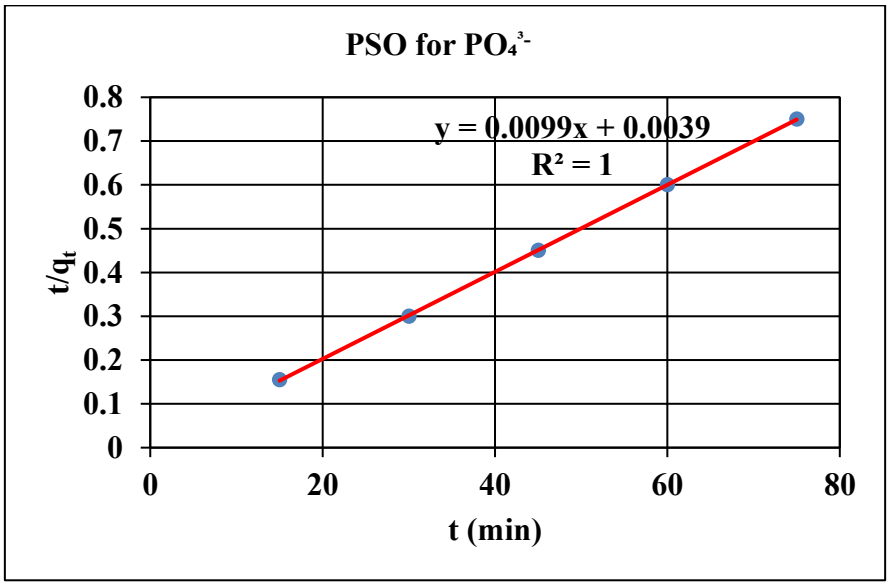

Figure 17: Pseudo-Second-Order parameters for phosphate (PO_4^{3-}) anion

4.4 Adsorption Thermodynamics studies for Phosphate (PO_4^{3-}) and Nitrate (NO_3^-) anions

A thermodynamic study analysis was conducted using the Van't Hoff plot (Figures 18 and 19) to understand the adsorption characteristics of phosphate (PO_4^{3-}) and nitrate (NO_3^-) anions on a magadiitic aluminosilicate nanozeolite respectively. The analysis (Table 14) revealed that the adsorption processes for both anions were endothermic ($\Delta H° > 0$) and entropy-driven ($\Delta S° > 0$). However, PO_4^{3-} ions exhibited strong spontaneity, confirmed by a highly negative Gibbs free energy $\Delta G° = -20.37$ kJ/mol at 25 °C (298 K), where the significant positive entropy changes …$\Delta S° = +207.85$ J/mol·K dominated the endothermic enthalpy $\Delta H° = +41.57$ kJ/mol, suggesting substantial structural reorganization due to ion desolvation, and the release of water molecules [30], leading to near-complete (99+ %) adsorption. In contrast, NO_3^- adsorption was less spontaneous $\Delta G° = -6.11$ kJ/mol at 25 °C (298 K) and showed a smaller entropy change $\Delta S° = +62.36$ J/mol·K, suggesting less solvent disruption and weaker electrostatic attraction [27]. This overall analysis confirmed the nanozeolite preferentially adsorbed PO_4^{3-} through primarily entropy-driven mechanisms, making its removal efficient even at ambient temperatures, while NO_3^- binding was weaker and temperature-sensitive.

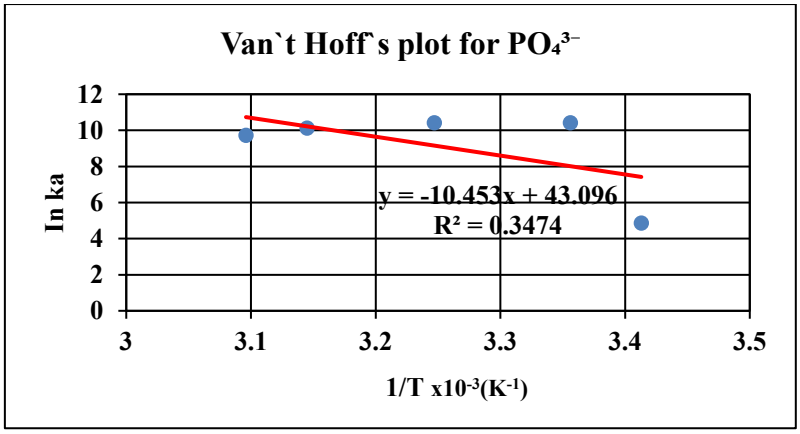

Figure 18: Van't Hoff adsorption Isotherm for phosphate (PO_4^{3-}) anion

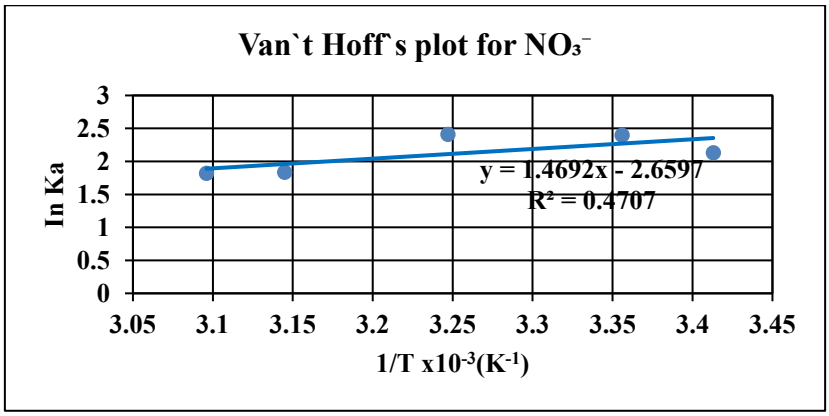

Figure19: Van't Hoff adsorption Isotherm for nitrate (NO_3^-) anion

Table 14: Van't Hoff analysis for the adsorption of PO_4^{3-} and NO_3^- anions

Parameter	PO_4^{3-} Adsorption	NO_3^- Adsorption
ΔH° (kJ/mol)	+41.57	+12.47
ΔS° (J/mol·K)	+207.85	+62.36
ΔG° (kJ/mol, 298 K)	-20.37	-6.11

5. CONCLUSION

The research successfully achieved its objective of determining the efficiency of Magadiitic aluminosilicate nanozeolites in the removal of agro-pollutants NO_3^- and PO_4^{3-}. The findings unequivocally demonstrate that the nanozeolite material exhibits superior efficiency and high selectivity for phosphate (PO_4^{3-}), making it an exceptional candidate for remediation efforts. Phosphate removal was remarkably robust, consistently achieving removal efficiencies exceeding 99.9 % across initial concentrations ranging from 5 mg/L to 50 mg/L, and exhibiting strong stability across the stable pH range of 2–6 and temperatures up to 35 °C. This high performance was fundamentally linked to strong chemisorption mechanisms, such as ligand exchange and inner-sphere complexation, characterized by an exceptionally high maximum adsorption capacity (q_m) of up to 2,736 mg/g and a highly spontaneous (ΔG° = -20.37 kJ/mol at 25 °C) and entropy-driven thermodynamic profile. Furthermore, the kinetics for PO_4^{3-} were

best described by the Pseudo-Second-Order (PSO) model, which confirmed chemisorption as the primary rate-limiting mechanism. In contrast, nitrate (NO_3^-) removal proved significantly less consistent and efficient, ranging between 65.88 % and 71.6 % across changes in concentration. Nitrate adsorption displayed high sensitivity to environmental variables, particularly declining sharply at pH levels above 6 and temperatures exceeding 35 °C. Mechanistic analysis confirmed that NO_3^- uptake was predominantly a physisorption-driven process supported by weaker electrostatic attractions, indicated by a low mean adsorption energy (E) of 3.45 kJ/mol and a less spontaneous nature ($\Delta G°$ = -6.11 kJ/mol at 25 °C) compared to phosphate. Recognizing that excess nitrate and phosphate are primary drivers of eutrophication and significant human health risks like methemoglobinemia, the successful application of the magadiitic aluminosilicate nanozeolite, particularly for phosphate removal, supports the goals of sustainable agriculture and provides an effective, cost-efficient solution for minimizing environmental pollution. To further enhance overall water purification, future research should focus on surface modification techniques to improve the binding capacity and selectivity of the magadiitic aluminosilicate nanozeolite for the monovalent nitrate anion.

Disclosure Statement

The authors declare no conflict of interest.

Acknowledgements

The authors would like to acknowledge the Technical staffs, at the Kericho Tea Research Institute for their support on liquid sample analysis. Also, thank the staff at the Department of Chemistry, University of Nairobi where this analysis was conducted. Again, acknowledge AI tool ChatGPT which was used to support the writing of this research.

REFERENCES

[1] Gabriel A. Waswa., Immaculate N. Michira., Deborah A. Abong'o., Dickson M. Andala., Austin O. Aluoch., (2020). "Characterization; formulation and application of Natural Nano zeolitic materials from Kenya as Smart Delivery Systems for fertilizers and pesticides", *International Journal of Scientific Research in Science, Engineering and Technology*, 7 (3), 338-349.

[2] Ward J., Parkin B., Powell J., & Smith G. (2018). The misuse and appropriation of subjective cognitive decline. *The Lancet Neurology*, 17 (11), 962–963

[3] Muralikrishna I. & Manickam, V. (2017). Environmental Management: Science and Engineering for Industry consists. *Science Direct*, Chapter 1, pg 1-4

[4] Zhang L, Wen Y., Zhiyong X., Guanqiang C., Wenying M. & Weihai X., (2020). Bioaccumulation and changes of trace metals over the last two decades in marine organisms from Guangdong coastal regions, South China, *Journal of Environmental Sciences,* 98:103-108

[5] World Health Organization and UNICEF, Progress on Sanitation and Drinking-Water, World Health Organization, Geneva, Switzerland, 2013

[6] Schoonheydt R.A., Geerlings P., Pidko E.A. & van Santen R.A. (2012). The framework basicity of zeolites. *J. Mater. Chem*., 22, 18705–18717.

[7] Oliveira D.S., Lima R.B., Pergher S.B.C. & Caldeira V.P.S. (2023). Hierarchical Zeolite Synthesis by Alkaline Treatment: Advantages and Applications. *Catalysts*, *13*:316

[8] Yi L., Lin L & Jihong Y., (2017). Applications of Zeolites in Sustainable Chemistry, *Natural materials* 3:928-949

[9] Bhatnagar A., & Sillanpää M. (2011). A review of emerging adsorbents for nitrate removal from water. *Chemical Engineering Journal, 168*(2), 493–504

[10] Yao, Y., Gao, B., Chen, J., Zhang, M., Inyang, M., Li, Y., Alva, A., & Yang, L. (2013). Engineered carbon (biochar) prepared by direct pyrolysis of Mg-accumulated tomato tissues: Characterization and phosphate removal potential. *Bioresource Technology*, 138, 8–13.

[11] Kumar A., Zhang S., Liu Y., Sun K., Sharma G., Naushad M., & Stadler F. J. (2021). Phosphate removal by La-modified zeolites: Mechanisms and efficiencies. *Journal of Hazardous Materials*, 403, 123805.

[12] Hussain S., Aziz H. A., Isa M. H., & Adlan M. N. (2017). Application of layered double hydroxides for removal of oxyanions: A review. *Water Research*, 124, 1-12.

[13] Wang L., Chen X., Zhang Y., Liu J., Tanaka K., Li F., Yang J., Wang S., Chen J., Zhou H., Liu Y., & Ok Y. S. (2022). Nitrate adsorption on metal oxides: Role of surface hydroxyl groups and pH-dependent mechanisms. *Environmental Science & Technology*, 56(5), 2987-2996.

[14] Awual M. R., Hasan M. M., Islam A., Rahman M. M., Asiri A. M., Khaleque M. A., & Sheikh M. C. (2019). Off-the- shelf visual nanoliter-scale nitrate meter based on fluorescent ligand-immobilized hybrid anion exchanger.*Chemical Engineering Journal*, 368, 21-28

[15] Omoko J. B., Njomo Njagi. Abong`o D. A., Andala D. M. (2025). Development and characterization of magadiitic aluminosilicate nanozeolite adsorbent using Magadi salt from Lake Magadi, Kenya. *International Journal of Research in Engineering, Science and Management*, Vol. 8 no. 10 pp 20-24.

[16] Langmuir I. (1918). The adsorption of gases on plane surfaces of glass, mica and platinum. *Journal of the American Chemical Society*, 40(9), 1361–1403

[17] Freundlich H.M. (1906). Over the Adsorption in Solution. *Journal of Physical Chemistry*, 57: 385-470.

[18] Temkin M. J. & Pyzhev V. (1960). Recent modifications to Langmuir isotherms, *Acta Physicochimica USSR*, 12: 217-222

[19] Dubinin M. M. & Radushkevich G. A. (1947). Mathematical equations describing the sorption of gases by solids. Zeitschrift für Physikalische Chemie, 255(3-4), 125-144

[20] Lingling L., Xu-Biao L., Lin D. & Sheng-Lian L., (2019). Application of Nanotechnology in the Removal of Heavy Metal from Water, Editor(s): Xubiao Luo, Fang Deng, In Micro and Nano Technologies, Nanomaterials for the Removal of Pollutants and Resource Reutilization, Elsevier, Pages 83-147

[21] Ho Y. S., & McKay G. (1999). *Pseudo-second-order model for sorption processes. Process Biochemistry*, *34*(5), 451–465

[22] Sparks, D. L. (2003). Environmental soil chemistry (2nd ed.). Academic Press.

[23] Borah D. K. & Bera M. (2004). Water shade-scale hydrologic and non-point source pollution models: review of applications. *Transactions of ASAE,* 47: 789-803

[24] Loganathan P., Vigneswaran S., Kandasamy J., & Naidu R. (2014). Defluoridation of drinking water using adsorption processes. *Journal of Colloid and Interface Science*, 418, 216–224.

[25] Maliyekkal S. M., Shukla S., Philip L., & Nambi I. M. (2013). Enhanced fluoride removal from drinking water by magnesia-amended activated alumina granules. *Separation and Purification Technology*, 117, 46-53

[26] Wang, S., Gao, B., Li, Y., Zimmerman, A. R., & Cao, X. (2015). Sorption of Cu (II) by biochars derived from six crop straws. *Bioresource Technology, 192*, 253–259.

[27] Huang Y., Lee X. Grattieri M., Yuan M., Cai R., & Macazo F. C. (2020). Modified biochar for phosphate adsorption in environmentally relevant conditions. *Chemical Engineering Journal,* 380, 122375

[28] Omoko J. B., Njomo Njagi, Abong`o D. A., Andala D. M. (2026). Adsorption Isotherms, Kinetics and Thermodynamics Studies of Lead, Chromium and Cadmium Removal Efficiency from Aqueous Solution Using Magadiitic Aluminosilicate Nanozeolite", *Int J Sci Res Sci Eng Technol*, vol. 13, no. 1, pp. 127–149, Jan. 2026, doi: 10.32628/IJSRSET26139.

[29] Chen L., Zhao X., Pan B., Zhang W., Hua M., Lv L., & Zhang Q. (2016). Preferable removal of phosphate from water using hydrous zirconium oxide-based nanocomposite of high stability. *Journal of Hazardous Materials*, 303, 17-24.

[30] He J., Zhang Y., Wang F., Zhou Y., & Liu L. (2020). Efficient removal of nitrate from water using amine-grafted agricultural waste-derived biochar: Preparation, characterization, and mechanism. *Environmental Science and Pollution Research*, 27(18), 22918-22931

[31] Foo K. Y. & Hameed B. H. (2019). Insights into the modeling of adsorption isotherm systems. *Chemical Engineering Journal*, 156(1), 2-10.

[32] Wang S. & Peng Y., (2010). "Natural zeolite as effective adsorbent in water and wastewater treatment. *Chemical Engineering Journal*, 156:11-24

[33] Crini G., Lichtfouse E., Wilson L. D., & Morin-Crini N. (2019). Conventional and non-conventional adsorbents for wastewater treatment. *Environmental Chemistry Letters,* 17(1), 145-155.